Composites: Part A 177 (2024) 107938

Contents lists available at ScienceDirect

Composites Part A

journal homepage: www.elsevier.com/locate/compositesa

A numerical model to prevent the thermal degradation of CFRPs at extreme heating rates – The laser processing of CF/PEEK

Dimitrios Gaitanelis [a,b,*], Chris Worrall [c], Mihalis Kazilas [d]

[a] Advanced Manufacturing Research Centre with Boeing, University of Sheffield, Catcliff, Rotherham S605TZ, United Kingdom
[b] NSIRC, TWI Ltd, Granta Park, Great Abington, Cambridge CB216AL, United Kingdom
[c] Advanced Composites and Adhesives Section (ACA), TWI Ltd, Cambridge CB216AL, United Kingdom
[d] Brunel Composites Centre (BCC), Brunel University London, Uxbridge UB83PH, United Kingdom

ARTICLE INFO

Keywords:
A. Polymer-matrix composites (PMCs)
A. Thermoplastic resin
C. Finite element analysis (FEA)
E. Heat treatment
Thermal degradation

ABSTRACT

This study proposes a coupled thermal-chemical numerical model for preventing the thermal degradation of carbon fibre (CF) reinforced polymers at extreme heating rates. Its applicability is demonstrated in a laser-heating case study of CF-reinforced poly-ether-ether-ketone (CF/PEEK). The kinetic parameters of the PEEK matrix, derived from thermogravimetric analysis at conventional heating rates, are introduced in the model and an extrapolation approach is applied to investigate the laser heating of CF/PEEK. The results show that the model captures the heating rate effect on the decomposition of the material, and is used to identify the processing conditions that can reach high temperatures without triggering the thermal degradation mechanisms of the PEEK matrix. Then, a multi-technique experimental investigation takes place to identify the processing conditions that first trigger the thermal degradation mechanisms of CF/PEEK in the examined laser-heating case study. Interestingly, a good agreement is found between the experimental and numerical investigations which validates the model and the applied extrapolation approach.

1. Introduction

The general advances in fast manufacturing technologies have increased the interest of both industry and academia in the laser processing of carbon fibre-reinforced polymers (CFRPs). Laser joining [1–5] and laser cutting [6–10], as flexible non-contact processes where localised heating is applied, have several benefits in the fields of composite/metal joining and composite machining. Significant research also takes place to further improve applications such as laser-assisted tape placement (LATP) due to the fast production rates that they can achieve [11–16]. One of the main damage mechanisms that can take place in these high-temperature applications is the thermal degradation of the polymer matrix. Thermal degradation could lead to mechanical properties deterioration and porosities formation [17–20]. Especially the porosities can significantly affect the post-processing structural integrity of the composite material, and of the composite/metal joint by causing delamination [1,21,22]. Therefore, one of the main goals in the laser processing of CFRPs is to identify the processing conditions that can ensure the required temperatures without activating the degradation mechanisms of the polymer matrix [23,24].

In many applications where laser heating is involved, such as laser joining or laser cutting, the common practice to reduce the heat-affected zone (HAZ) is to proceed to an optimisation process that takes place experimentally [1,2,6,7,18,25]. Considering the increased cost and complexity of this process, the use of cost-effective methods such as finite element analysis (FEA) offers an interesting alternative [26,27]. Aligned with that, this study proposes a numerical framework that can identify the processing conditions that can prevent the thermal degradation mechanisms of CFRPs at extreme heating rates, and the applicability of the model is demonstrated in a laser heating case study of CF-reinforced poly-ether-ether-ketone (CF/PEEK).

So far, several studies have examined numerically the laser heating of CF/PEEK [28–30] as well as its laser joining applications with metals [18,31]. In addition, mathematical models have been developed to examine the heat distribution of CF/PEEK during laser ablation [32]. Commonly, temperature-dependent material properties are considered to examine the response of CF/PEEK in these conditions. Nevertheless, research has shown that the heating rate influences the response of the material and offsets its decomposition at higher temperatures as the heating rate increases [33,34]. Hence, it is important to consider the

* Corresponding author at: Advanced Manufacturing Research Centre with Boeing, University of Sheffield, Catcliff, Rotherham S605TZ, United Kingdom.
E-mail address: d.gaitanelis@sheffield.ac.uk (D. Gaitanelis).

https://doi.org/10.1016/j.compositesa.2023.107938
Received 26 July 2023; Received in revised form 23 October 2023; Accepted 29 November 2023
Available online 2 December 2023

heating rate effect to accurately capture the response of CF/PEEK in laser processing.

An effective methodology accounting for this effect involves the use of an extrapolation approach. This approach utilises the kinetic model of the matrix material - as derived from thermogravimetric analysis (TGA) at conventional heating rates – to examine the material's response at extreme heating conditions. It has been recently used in lightning strike studies of CFRPs as an alternative to using temperature-dependent material properties [35–39]. Interestingly, Millen et al. showed that using an extrapolation approach improves the damage predictions in lightning strike simulations and reduces the error in predicting the severe damage area to within 8 % of the experimental values [40]. Therefore, it could also be relevant for a range of high-temperature applications of CFRPs where the main objective is to reduce the HAZ of the material, and this work utilises this approach to identify the laser processing of CF/PEEK that slightly triggers the thermal degradation mechanisms of the PEEK matrix.

Consequently, another important objective of this study is to validate the applied extrapolation approach. In general, a suitable test setup where it would be possible to examine the decomposition of polymers and composites at extreme heating rates is not available yet. For example, the maximum heating rate of conventional TGA equipment is limited to a few hundred °C/min, while the material experiences a heating rate $\geq$ 10,000 °C/min during laser heating or lightning strike phenomena [40]. Hence, the validity of the applied extrapolation approach cannot be directly assessed, and to address this issue attenuated total reflection-Fourier transform infrared spectroscopy (ATR-FTIR) is employed in this work as an alternative methodology. ATR-FTIR can detect the processing conditions that initially trigger the thermal degradation mechanisms of CF/PEEK, and thus it can also be used to assess the validity of the applied extrapolation approach.

Altogether, the calculated kinetic model of PEEK at conventional heating rates is introduced in Abaqus software with the user-defined subroutines HETVAL and USDFLD [41], and an extrapolation approach is applied to examine the response of CF/PEEK in laser heating. Through this process, the power density that slightly triggers the decomposition mechanisms of the PEEK matrix is defined for both a Gaussian and a top-hat laser beam. To validate the model, an experimental investigation takes place where the laser-heated samples are examined with ATR-FTIR and optical microscopy (OM), and their surface roughness and surface morphology are also assessed. Interestingly, a good agreement is reached between the two investigations regarding the critical laser power that first triggers the thermal degradation mechanisms of CF/PEEK. This is a significant finding since it provides evidence for the first time that the applied extrapolation approach manages to capture the onset of degradation in the extreme heating conditions that take place in laser heating. Taken together, this paper is structured as follows: Section 2 describes the theoretical background of the proposed numerical framework. Section 3 focuses on the derived kinetic model and discusses the applied extrapolation approach, while the main outputs of the numerical and the experimental investigation are presented in Section 4 and Section 5 respectively. Finally, the main conclusions of the study are gathered in Section 6.

2. Theoretical background

When CFRPs are subjected to extreme heating conditions, various physical and chemical phenomena occur, and thermal-chemical–mechanical coupling effects take place. First, the increased temperatures result in the degradation of the polymer matrix which leads to the diffusion of decomposition gases and variations in the material properties [42]. Foster et al. successfully described the pattern that leads to thermally induced damage in CFRPs at extreme heating conditions [43]. The as-received material has a significantly higher conductivity in the longitudinal fibre direction than in its transverse and through-thickness direction. Therefore, the greatest part of the applied heat flux will first flow through its fibre direction. As the heating process develops and the decomposition of the polymer matrix occurs, proportionally more heat will flow in the other two directions of the material [43]. Likewise, a similar heating sequence will take place in the adjacent plies resulting in the overall heat-affected region of the CFRP.

As far as modelling is concerned, to capture the thermal behaviour of the composite material as decomposition progresses it is important to realistically represent its properties. The properties of the decomposing material and the properties before and after decomposition must be considered. To do so, the decomposition degree α is defined where

$$\alpha = \left[\frac{\rho_{virgin} - \rho}{\rho_{virgin} - \rho_{charred}}\right] \tag{1}$$

In Eq. (1), ρ_{virgin} and $\rho_{charred}$ represent the virgin and the charred state of the material density, while ρ is the instant density. After defining the decomposition degree α, the common practice is to consider the properties of the decomposing material as being dependent on the relative fractions of its char and its virgin state [19,35,38,42]. For example, the thermal conductivity k_{xx} in the x direction and the specific heat C_p of the decomposing material can be described by

$$k_{xx} = \alpha k_{xx}^{charred} + (1-\alpha)k_{xx}^{virgin} \tag{2}$$

$$C_p = \alpha C_p^{charred} + (1-\alpha)C_p^{virgin} \tag{3}$$

respectively. As seen in Eqs. (2) and (3), the decomposing material's properties are dependent on the corresponding properties of the material at its virgin (k_{xx}^{virgin}, C_p^{virgin}) and charred state ($k_{xx}^{charred}$, $C_p^{charred}$). To describe the coupled thermal-chemical behaviour of CFRPs in laser heating Eq. (4) is commonly applied [44]:

$$\rho C_p \frac{\theta T}{\theta t} = \nabla(k\nabla T) + Q_{Laser} - \rho H_s \frac{d\alpha}{dt} \tag{4}$$

where ρ, C_p, and k represent the density (kg/m^3), the specific heat (J/kg·K), and the thermal conductivity of the material (W/m·K), while Q_{Laser} represents the absorbed energy from the laser (W/m^2) and H_s the reaction heat due to the matrix decomposition (J/g·s). The latter value is defined with pyrolysis combustion flow calorimeter (PCFC) testing and equals 302 J/g·s for pure PEEK [45]. Finally, the rate of the decomposition degree over time can be expressed as the n-th power of the non-decomposed material [46], as shown by

$$\frac{d\alpha}{dt} = K(T)(1-\alpha)^n \tag{5}$$

where $K(T)$ is the kinetic model defined by:

$$K(T) = A\exp\left(\frac{-E_a}{RT}\right) \tag{6}$$

In the Arrhenius-type Eq. (6), R is the universal gas constant (8.3145 J/mol·K) while A, E_a, and n are the pre-exponential factor (1/s), the activation energy (kJ/mol), and the reaction order respectively. These parameters are commonly calculated from TGA experiments at conventional heating rates. Regarding their numerical implementation, Abaqus/standard finite element code does not incorporate the described theoretical foundation. Hence, to introduce the kinetic model of PEEK in the solver, the user-defined subroutines USDFLD and HETVAL are used and the integrated form of Eq. (5) ($t = 0$, $\alpha = 0$) is implemented with:

$$\alpha = 1 - \left[(n-1)Aexp\left(\frac{-E_a}{RT}\right)t + 1\right]^{\frac{1}{1-n}} \tag{7}$$

Eq. (7) calculates the decomposition degree field throughout the simulation by applying the Scheil superposition principle. This principle was first introduced by Hildenwall et al. [47], and is commonly used when non-isothermal phase changes occur [35,36]. Numerically, it is based on time discretization and assumes that degradation is an

isothermal process in the time increment Δt, which is a lot shorter than the total time of the phenomenon. Taken together, the final equations that are used for calculating the decomposition degree field are represented by

$$\begin{cases} \alpha_1 = 1 - \left[(n-1)Aexp\left(\dfrac{-E_a}{R(T_1+T_0)/2}\right)t_1 + 1\right]^{\frac{1}{1-n}} \\ \alpha_i = 1 - \left[(1-\alpha_{i-1})^{1-n} + (n-1)Aexp\left(\dfrac{-E_a}{R(T_{i-1}+T_i)/2}\right)\Delta t\right]^{\frac{1}{1-n}} (i \geq 2) \end{cases} \quad (8)$$

The first part of Eq. (8) calculates the decomposition degree α_1 in the initial step. When $i \geq 2$, the value of α_i in each step is consequently derived considering the decomposition degree of the previous step, α_{i-1}, and the temperature values in the time increment Δt. With this methodology, the PEEK kinetics are implemented in the model and the decomposition degree field is captured throughout the simulation. Its values are then used as a field variable with the user-defined subroutine USDFLD to update the material properties of the examined CFRP in each increment. Hence, the exact material state is considered throughout the simulation, and overall a coupled thermal-chemical analysis is carried out where a decomposition dependency of the material properties is established.

3. Kinetic model and applied extrapolation approach

The Kinetics Committee of the International Confederation for Thermal Analysis and Calorimetry (ICTAC) recommends slower heating rates for deriving the kinetic model of polymers and composites. The reason for this is that faster heating rates can result in implications between the accurate measurement of the sample's mass and of the reference temperature that is captured with the thermal analysis instruments [48]. Therefore, PEEK samples of 7.6 mg ± 0.6 mg are examined in an air atmosphere at heating rates of 2.5, 5, and 10 °C/min using a TGA 2 thermogravimetry from Mettler Toledo. Fig. 1a shows that the decomposition of PEEK takes place in two steps [34,49]. In this work, the focus is given to the first decomposition step where the material could still maintain part of its structural integrity (Fig. 1a). To calculate the kinetic parameters of PEEK, the Ozawa/Flynn/Wall method [50] is applied (Fig. 1b) in accordance with the ASTM Standard E1641 [51]. The analysis of the first decomposition step captures a pre-exponential factor A equal to 4.27×10^{13} (1/sec), an activation energy E_a equal to 182.09 kJ/mol and a reaction order n equal to 2.2, which agree with the results of previous studies that examined the decomposition of PEEK at similar heating conditions [33].

These parameters are introduced in Abaqus software with the user-defined subroutine HETVAL, and an extrapolation approach is applied to examine the response of CF/PEEK in laser heating. To present an initial validation of the applied extrapolation approach, Fig. 2 shows the extrapolated response of PEEK's kinetic model at 100 °C/min, along with its experimental curve at the same heating rate. This is the maximum heating rate achieved with the available equipment, and the analysis indicates a very good agreement between the experimental results and the kinetic model's calculation at 100 °C/min. Fig. 2 also illustrates how an increased heating rate offsets the decomposition of the material at even higher temperatures. For example, the temperature where 5 % of the initial mass is lost ($T_{95\%}$) increases from 597 °C at 100 °C/min to 729 °C at 10^6 °C/min, as calculated by the kinetic model. To account for this effect, temperature offsets have been previously used in lightning strike studies to estimate more realistically the thermal damage of CFRPs at these conditions [40,43,52]. Nonetheless, as shown in section 4.2, the proposed numerical framework can capture the heating rate effect on the decomposition of the material which is an important benefit in applications where extreme heating rates are applied.

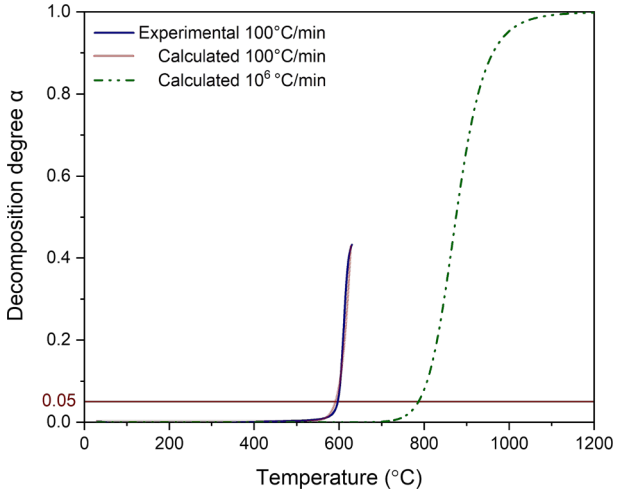

Fig. 2. Validation of the kinetic model with experimental data at 100 °C/min (first decomposition step) and predicted decomposition of PEEK when heated at 10^6 °C/min.

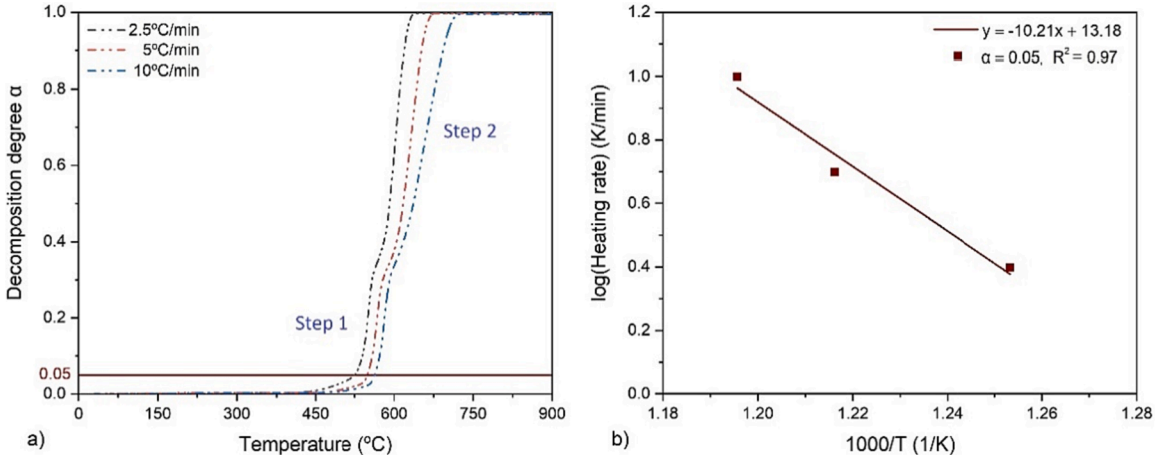

Fig. 1. (a) Decomposition degree α versus temperature of the TGA experiments of PEEK in air at 2.5, 5, and 10 °C/min, and (b) logarithm of the heating rate versus 1000/Temperature when α is equal to 0.05.

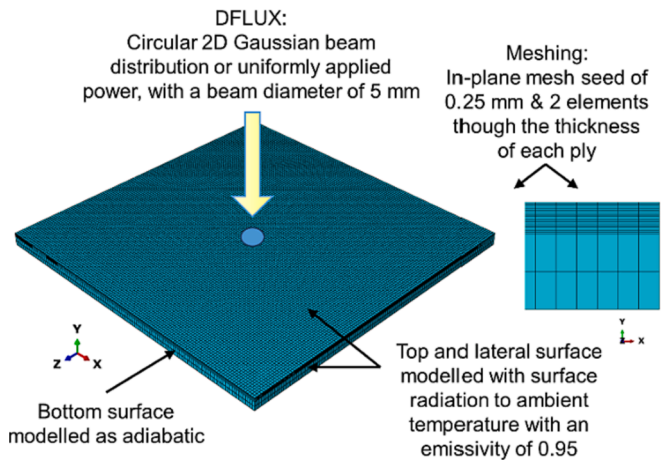

Fig. 3. Numerical model characteristics: Boundary conditions, applied heat flux, and mesh characteristics.

4. Numerical investigation

The laser-heated samples are modelled in Abaqus® software and a two-step transient heat transfer analysis is carried out. In the first step, the applied heat flux is simulated and in the second step the resulting heat dissipation is modelled for a maximum of three seconds. This duration is found sufficient for modelling the heat dissipation through the thickness of the CF/PEEK laminate. For each set of processing parameters, a panel of 100 mm × 100 mm × 4 mm is simulated and the top eight plies follow the stacking sequence described in section 5.1. The rest of the laminate is divided into eight parts that follow a $[0°/90°]_4$ stacking sequence. Two elements are considered through the thickness of the top eight plies, and the model is meshed with 8-node linear heat transfer brick solied elements (DC3D8) (Fig. 3). The boundary conditions aim to reproduce the experimental process, and surface radiation is considered on the top and the lateral surfaces while the bottom surface is modelled as adiabatic. Finally, the laser beam is modelled as a circular two-dimensional (2D) Gaussian beam or as a top-hat laser beam over the x–z plane on the centre of the top surface with subroutine DFLUX (Fig. 3). The exact equation of the applied heat flux, Q_{Laser}, is described by

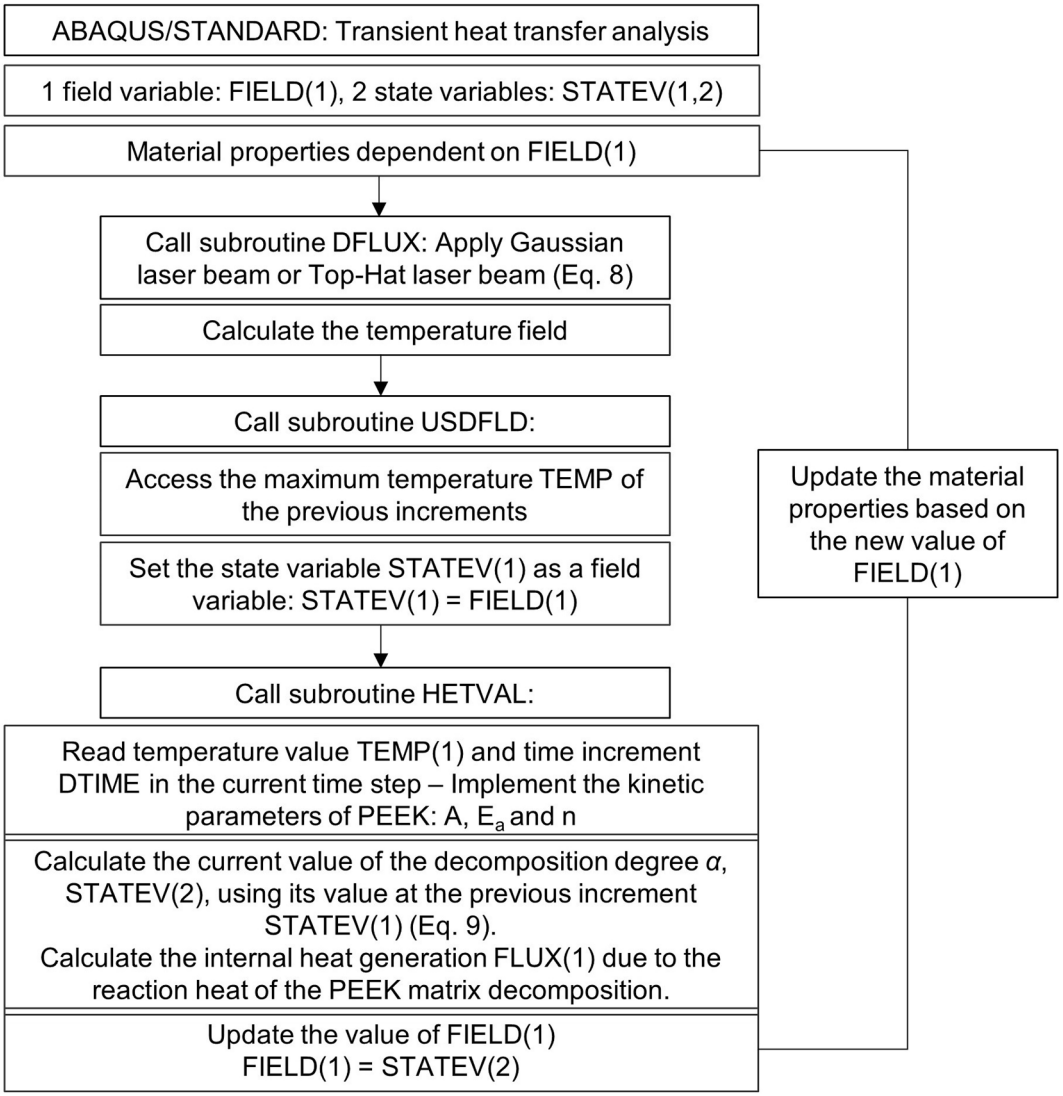

Fig. 4. Schematic figure of the model with the implemented subroutines: DFLUX, USDFLD & HETVAL.

Table 1
Decomposition-dependent material properties of CF/PEEK [53–55] and calculated kinetic parameters of PEEK that are implemented in the model.

Decomposition-dependent material properties of CF/PEEK					
Decomposition degree α	Density (kg/m^3)	Specific heat (J/kg·K)	Thermal conductivity (W/m·K)		
			Longitudinal	Transverse	Through-thickness
0	1590	823	4.1	0.47	0.47
1	1270.4	2171	1.736	0.1	0.1
Calculated kinetic parameters of the PEEK matrix					
Activation energy E_a (kJ/mol)		Pre-exponential factor A (1/sec)		Reaction order n	
182.09		4.27×10^{13}		2.2	

$$\begin{cases} Q_{Laser}^{Gaussian} = \dfrac{2P_{Laser}}{\pi r_{Laser}^2} exp\left[-2\left(\dfrac{(x-x_0)^2 + (z-z_0)^2}{r_{Laser}^2} \right) \right] \\ Q_{Laser}^{Top-hat} = \dfrac{P_{Laser}}{\pi r_{Laser}^2} \end{cases} \quad (9)$$

for the Gaussian and the top-hat laser respectively where P_{Laser} is the laser power and r_{Laser} is the laser beam radius. Finally, the kinetic model of the PEEK matrix is implemented with the user-defined subroutines HETVAL and USDFLD and Fig. 4 presents a detailed schematic of the exact process.

Fig. 4 shows that the material properties are updated in each increment according to the calculated value of the decomposition degree α. Overall, the properties of the decomposing material are modelled to vary linearly with the decomposition degree from the virgin ($\alpha = 0$) to the charred state of the material ($\alpha = 1$). The exact decomposition- dependent material properties and the calculated kinetic parameters of PEEK can be seen in Table 1. The modelled properties of CF/PEEK prior to the onset of degradation are derived from experimental studies that took place at room temperature [53,54]. In the absence of experimental data for charred CF/PEEK, properties from the study of Griffis et al. [55] on charred AS4/3501-6 graphite epoxy are employed. Although the matrix material differs, it is considered appropriate for this study as the thermal properties at full matrix decomposition are mainly influenced by the intact reinforcement. To date, only a limited number of investigations have explored the properties of charred composites, and the existing studies are over 30 years old [55–57]. Consequently, more current studies that incorporate recent technological advancements would benefit the research community.

Taken together, the main objective of this work is to identify the laser heating that slightly triggers the decomposition mechanisms of the PEEK matrix. Nevertheless, the introduced numerical recipe can be applied to a wider range of heat transfer problems with even higher expected temperatures. Hence, when full decomposition occurs the charred properties from the study of Griffis et al. are applied in the model [55] and a char yield of 80 % is considered [58]. Finally, the sublimation of CF is modelled to take place from 3316 °C to 3334 °C and 43 kJ/g are assumed to be released as latent heat in that temperature window [56].

4.1. Applicability of the model in cases where full decomposition occurs (1600 W-10 ms)

First, a 2D Gaussian beam distribution with a laser beam diameter of 5 mm and an applied power of 1600 W for 10 ms is examined. The obtained temperature and decomposition degree field is illustrated in Fig. 5. The maximum temperature on the surface of the top ply reaches 3326 °C (Fig. 5a) and the decomposition degree α equals to one throughout the heated area (Fig. 5b). At these temperatures, fibre ablation occurs [65] and the PEEK matrix fully decomposes. Interestingly, scanning electron microscopy (SEM) captures these damage mechanisms when the CF/PEEK plate is laser heated with a Gaussian beam of a 5 mm spot diameter at these conditions (1600 W–10 ms) (Fig. 5e).

The cross-thickness temperature field is also examined, and Fig. 6 displays the temperature distribution of representative nodes located between the second and seventh ply at the centre of the applied laser beam. The T_g of PEEK is surpassed in all the plies apart from the seventh ply (Fig. 6). The high temperatures that are reached could potentially affect the cross-thickness crystallinity of the laminate and hence deteriorate its mechanical properties. Nonetheless, the short amount of time that the material remains at these temperatures does not guarantee a significant impact on the crystallinity content. However, the rapid heating and cooling that takes place during laser heating have been previously associated with the lower levels of crystallinity that are found in CF/PEEK structures made with LATP [59–61]. To determine whether the applied laser heating affects the cross-thickness crystallinity of CF/PEEK, a localised crystallinity assessment would be recommended that exceeds the scope of this study.

Regarding thermal degradation, Fig. 5d indicates that it is also triggered at the second ply of the laser-heated laminate. In this ply, the degraded area is limited in the centre of the heated region where the applied heat flux has its maximum value. As previously mentioned, since the thermal conductivity of CF/PEEK is significantly less in the through-thickness direction than in the longitudinal direction (Table 1), the resulting degradation is limited to the top two plies of the laminate. Likewise, the extent of degradation in the second ply (Fig. 5d) is significantly less than in the heated surface of the top ply (Fig. 5b).

4.2. The heating rate effect on the decomposition of PEEK as captured with the numerical model

Fig. 7 shows that the two degraded plies experience a significantly different decomposition process. In the first ply, degradation initiates around 825 °C and a 1 % mass loss takes place at 873 °C. On the other hand, in the second ply of the heated laminate 45 % of the initial mass has already decomposed at 787 °C (Fig. 7). The observed difference is due to the different heating rates that the two areas experience. For example, the top ply reaches a full decomposition within the first 10 ms

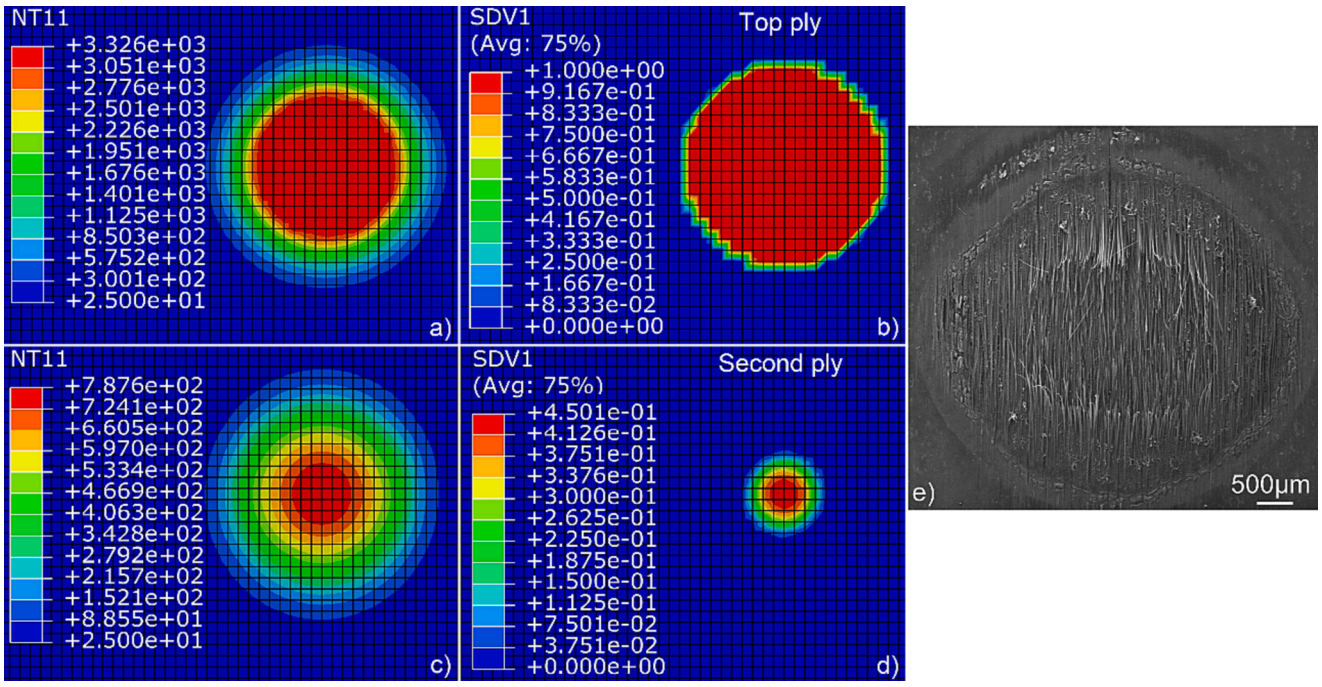

Fig. 5. Temperature (°C) and decomposition degree field as captured by the model when CF/PEEK is heated wth a Gaussian beam (1600 W–10 ms): (a-b) top ply, (c-d) second ply, and (e) laser-heated surface of CF/PEEK at the examined heating conditions.

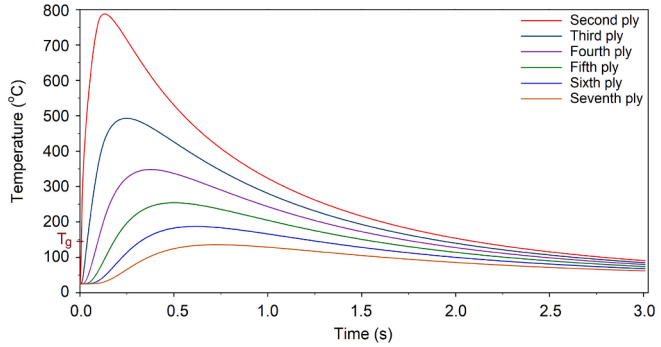

Fig. 6. Temperature profile of representative nodes in the in-depth direction (1600 W–10 ms).

of the applied laser heating. On the other hand, the second ply reaches its maximum temperature during the proceeding heat dissipation step and particularly 0.1328 s after the applied thermal load. Consequently, the two plies experience a heating process with significantly different heating rates, and indicatively the heating rate is 56 times greater in the first ply than in the second ply.

Altogether, Fig. 7 demonstrates that the developed methodology can capture the heating rate effect. Considering that the material properties are a function of the decomposition degree, this is an important advantage. With this approach, the properties of each element are updated based on its thermal history. For example, at 787 °C the second ply has already decomposed by 45 % while the first ply has not yet reached its onset of decomposition. Hence, the two elements are modelled with different material properties at 787 °C that correspond to the extent of degradation they have experienced at these temperatures.

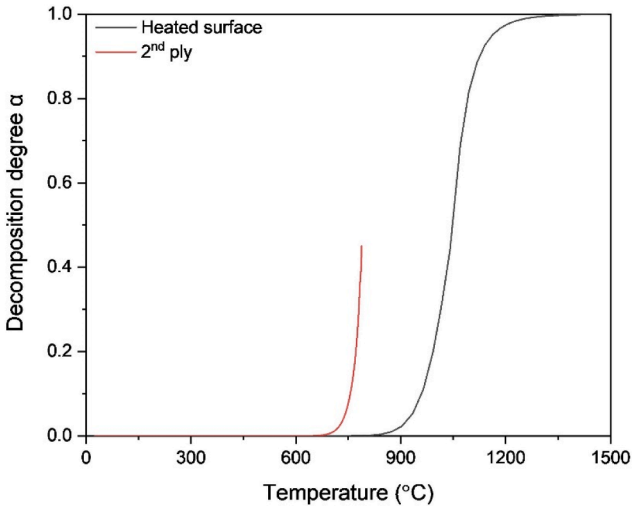

Fig. 7. Decomposition degree α versus temperature in the two degraded plies (1600 W–10 ms).

By considering the effect of the applied heating rate, this methodology ensures a more accurate representation of the material properties throughout the simulation compared to the use of temperature-dependent material properties, which is overall the main key for a successful model [42].

4.3. *Laser heating of CF/PEEK without the effects of degradation*

After presenting the capabilities of the model in power densities that

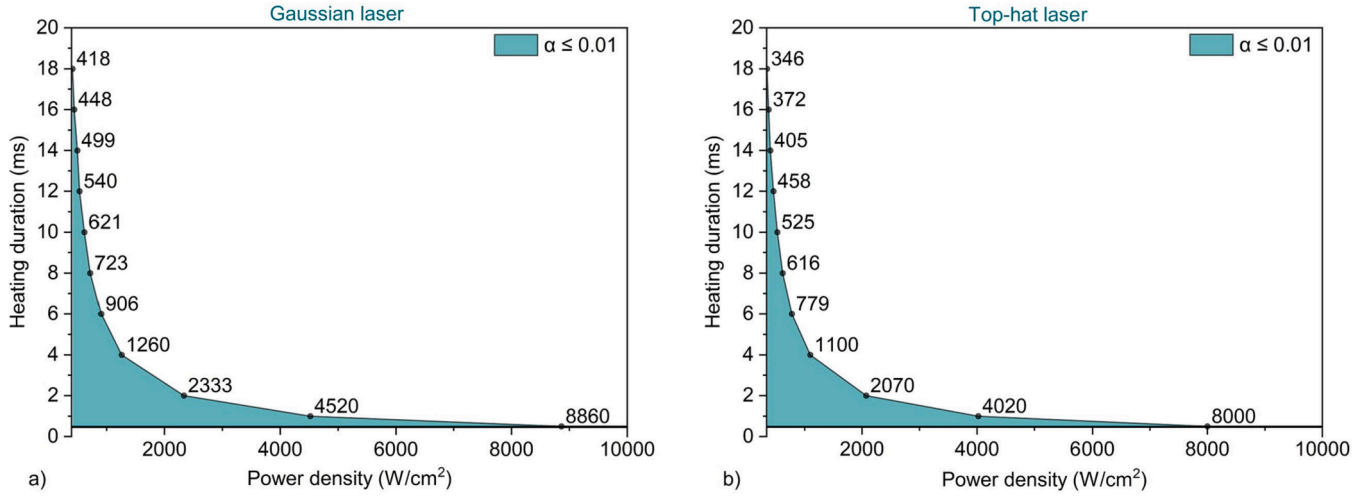

Fig. 8. Process window for achieving a decomposition of PEEK less than 1 % ($\alpha \leq 0.01$), when CF/PEEK is subject to laser heating with: (a) a 2D circular Gaussian laser beam, and (b) a top-hat laser configuration.

lead to full decomposition, the model is used to identify the processing conditions that do not severely decompose the material and can therefore achieve high temperatures without the consequences of thermal degradation. From a previous study by the authors, a decomposition of the PEEK matrix around 1 % was found tolerable and ensures a limited effect on the crystallinity content of CF/PEEK [34]. Likewise, several studies have set a decomposition equal to 1 % as the threshold that would ensure the required post-processing structural integrity of CF/PEEK after laser processing [62–64]. Hence, a value of α equal to 0.01 is considered in this study as the thermal limit of laser-heated CF/PEEK, and Fig. 8 presents the power density that leads to a decomposition of PEEK around 1 % ($\alpha \leq 0.01$) for a heating duration between 0.5 ms and 18 ms. According to the results of the model, the critical power density varies from 8860 W/cm^2 to 418 W/cm^2 when a Gaussian laser beam is applied and from 8000 W/cm^2 to 346 W/cm^2 when a top-hat laser beam is used.

5. Experimental investigation

To validate the model and the applied extrapolation approach, an experimental investigation takes place where the numerically examined CF/PEEK laminate is laser heated with a top-hat laser beam. An IPG YLS-5000 continuous wave (CW) fibre laser is used with a maximum power of 5000 W and a wavelength of 1070 nm. A beam of 8.1 mm spot diameter is applied on the surface of the examined specimens for a heating duration equal to 1 ms. The model captures a critical power density of 4020 W/cm^2 required to achieve a 1 % degradation in CF/PEEK when exposed to a top-hat laser beam for 1 ms (Fig. 8b). Thus, given the 8.1 mm spot diameter of the applied laser beam, the critical laser power that results in a 1 % decomposition equals 2070 W. To assess the validity of this result, several laser powers are applied to CF/PEEK within the range of 1500 W–3000 W.

One of the main challenges in high-temperature – short-duration processing is to measure experimentally the maximum temperatures that occur [49]. This is a difficult task, especially in applications where the applied heating only takes place for 1 ms. Conventional thermocouples have a response time that is significantly greater than that, which results in an underestimation of the measured temperatures. Additionally, even though optical pyrometry and infrared thermography are well-established techniques the existing difficulty in capturing the material's emissivity variations during the heating process can affect their maximum accuracy [65]. Nevertheless, even if the exact temperatures are captured they would not necessarily provide sufficient information for answering whether thermal damage is induced in the material [49].

For thermal damage to take place, both the reached temperatures and the dwell time at these temperatures are important. Especially in the exteme heating rates that are applied in laser heating, it is evident that the smaller amount of time that the polymer would remain at increased temperatures may not necessarily trigger the thermal degradation mechanisms of the heated material. Therefore, to optimise the applied high-temperature – short-duration processing or laser processing of CF/PEEK it is important to employ the appropriate techniques that could detect the event of thermal damage in the examined conditions [49,66]. In this study, ATR-FTIR is proposed as a method that could address this issue and it is used in this work for assessing the validity of the applied extrapolation approach. Altogether, the laser-heated specimens are examined with ATR-FTIR and OM and the laser power that initially triggers the thermal degradation mechanisms of CF/PEEK is identified and compared with the results of the numerical model. Additionally, to further examine the impact of laser heating on CF/PEEK the examined samples' surface morphology and surface roughness are assessed using a three-dimensional (3D) non-contact profilometer.

5.1. Examined material

The examined CF/PEEK laminate is manufactured at TWI Ltd., Cambridge, UK, and has a uniform stacking sequence of $[0°/90°/0°]_9$. Tenax®-E TPUD PEEK-HTS45 unidirectional (UD) prepregs were used with a nominal thickness of 0.14 mm provided by Teijin Limited. The manufacturing process took place in a hot press, where the 27 layers were initially heated from the top platen at 400 °C with an applied light contact for 30 min. Then, the pressure was set to 150 bar and the layers were slowly cooled to 100 °C, where the formed laminate was removed and let to naturally cool down to room temperature. The final dimensions of the plate were 280 mm × 280 mm × 4 mm.

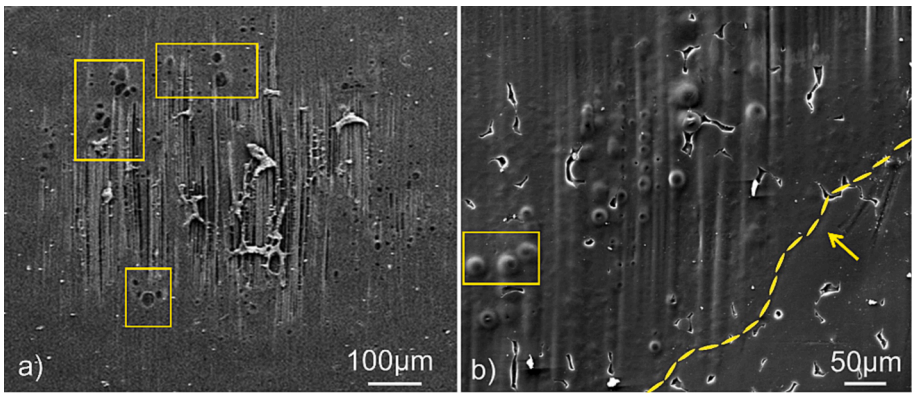

Fig. 9. Formed porosities on the surface of CF/PEEK after laser heating with (a) a Gaussian laser beam and (b) a top-hat laser beam.

5.2. Damage mechanisms on the surface of laser-heated CF/PEEK

As shown in Fig. 5e, at higher power densities fibre breakage and material ablation take place on the laser-heated surface of CF/PEEK. Interestingly, these damage types are also captured by the numerical model at the examined conditions (Fig. 5a, Fig. 5b). Another important damage mechanism that takes place at CF/PEEK upon laser heating is the occurrence of porosities. For example, formed porosities are evident when the material is heated with a Gaussian and a top hat laser beam (Fig. 9). Their main formation mechanism is the thermal degradation of the polymer matrix where the gaseous products that are produced eventually form the porosities [1] which can then lead to delamination [1,2,21]. Finally, after comparing the heat-affected region of the CF/PEEK specimens with their non-affected region, matrix decomposition, resin deterioration, and fibre exposure are also observed (Fig. 9). Similarly to this study, these damage mechanisms have been outlined in several experimental investigations available in the public domain literature [19,67].

5.3. ATR-FTIR analysis

A Nicolet iS50 FTIR spectrometer operating with the built-in diamond ATR from Thermo Fischer Scientific Inc. is used and the accumulated spectra are collected from 4000 to 600 cm^{-1} with a resolution of 4 cm^{-1} and a total of 128 scans. To proceed to the analysis, the accumulated spectra are baseline-corrected and normalised to the 1593 cm^{-1} peak [34,49]. As indicated with arrows in Fig. 10, changes are mainly noticed within the 1400–800 cm^{-1} spectral region of the laser-heated samples. A shoulder is detected on the proximal ether peak at 1216 cm^{-1} as well as changes in the diphenylether bonds around 1110 cm^{-1}. The intensity ratios of the 1305/1280 cm^{-1} and of the 966/952 cm^{-1} IR bands, and the aromatic hydrogens at 863 cm^{-1} and 841 cm^{-1} are also altered [34,49]. These changes are associated with the process of thermal degradation in CF/PEEK, and are attributed to the cross-linking mechanisms that take place in the PEEK matrix with the applied thermal load [68,69].

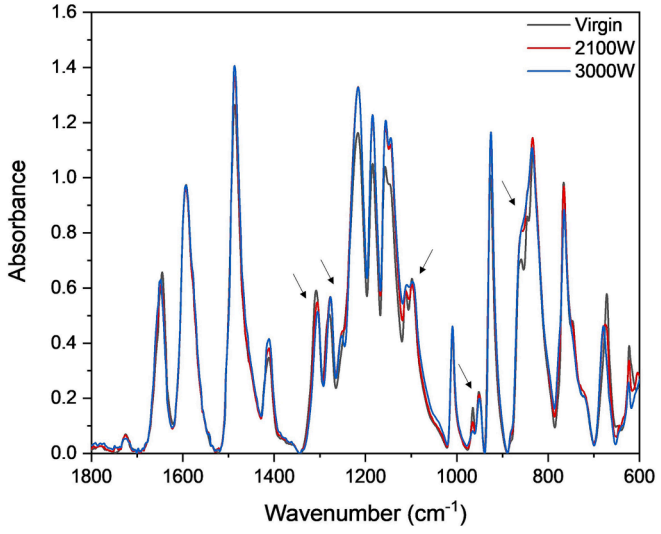

Fig. 10. IR spectra of CF/PEEK before and after the applied laser heating of 1 ms with a top-hat laser beam of 8.1 mm spot diameter and a laser power equal to 2100 W and 3000 W.

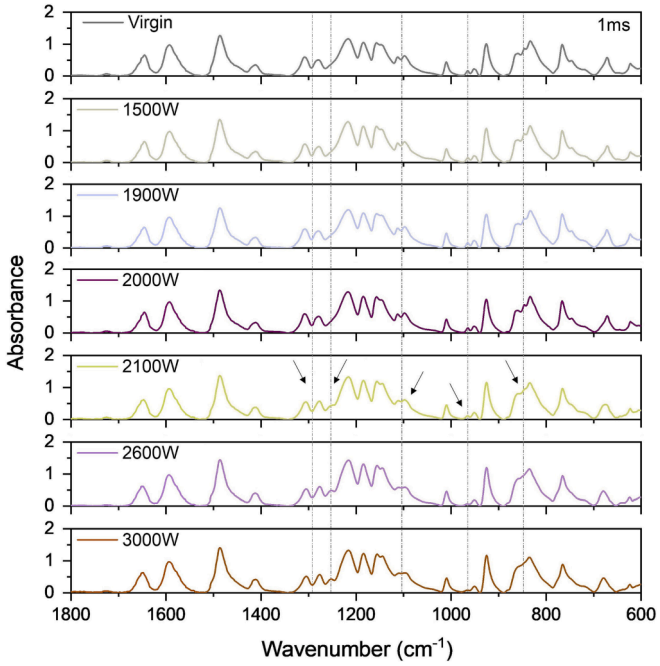

Fig. 11. IR spectra of virgin CF/PEEK, and laser-heated CF/PEEK with a top-hat laser beam of 8.1 mm spot diameter, a heating duration of 1 ms, and a power of 1500 W, 1900 W, 2000 W, 2100 W, 2600 W, and 3000 W.

5.3.1. Laser power that first triggers the thermal degradation of CF/PEEK

As already indicated, ATR-FTIR is a useful technique for following the spectral changes that occur in PEEK and CF/PEEK upon the event of thermal degradation [34,49,66]. Therefore, it is applied in this work to detect which processing conditions first trigger the degradation mechanisms of the laser-heated specimens. Fig. 11 shows that the spectral changes that are associated with the event of thermal degradation are first noticed in the specimen heated at 2100 W. When laser powers lower

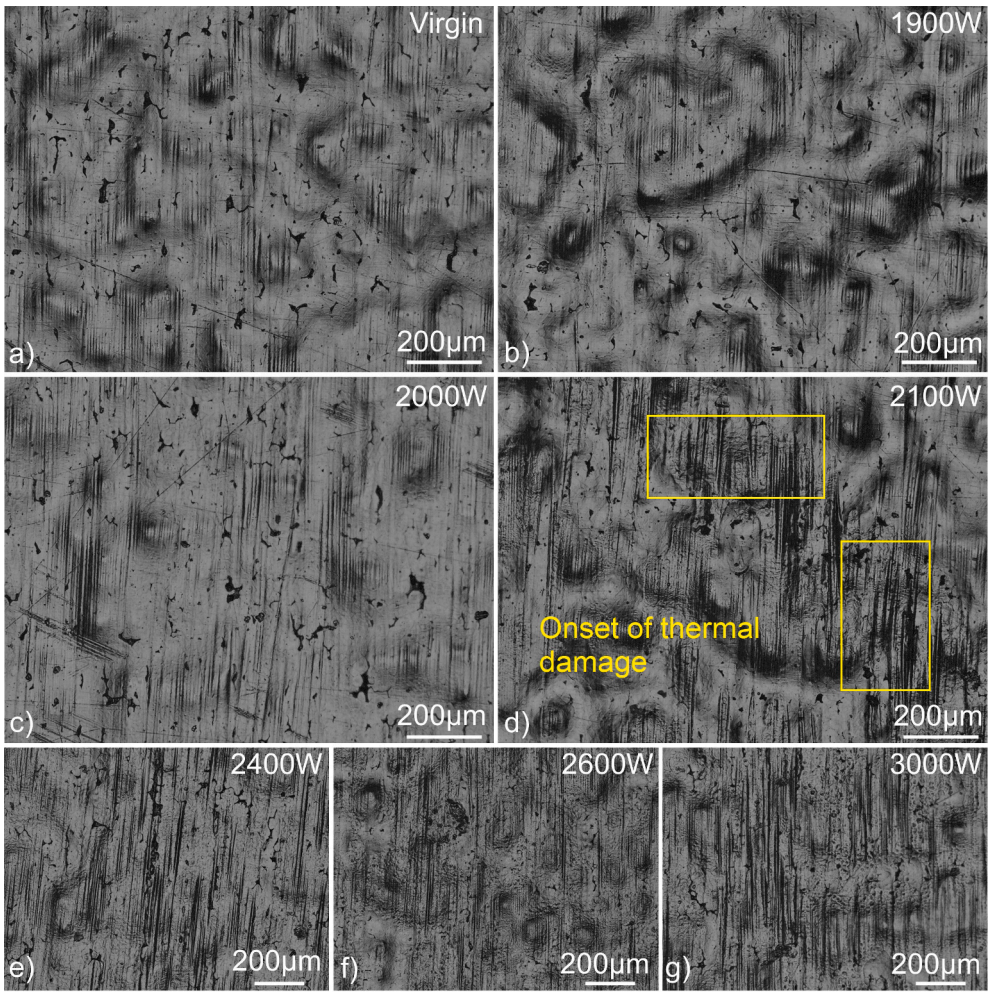

Fig. 12. Surface of: (a) virgin CF/PEEK, and of CF/PEEK after laser heating of 1 ms with a top-hat laser beam of 8.1 mm spot diameter and a power of (b) 1900 W, (c) 2000 W, (d) 2100 W, (e) 2400 W, (f) 2600 W, and (g) 3000 W.

than 2100 W are applied, the accumulated spectra are similar to the spectra of the as-received CF/PEEK, indicating that thermal degradation has not taken place in these conditions (Fig. 11). On the other hand, spectral changes at 1253 cm^{-1}, 1100 cm^{-1}, 970 cm^{-1} and 850 cm^{-1} and in the 1305/1280 cm^{-1} intensity ratio are detected in the samples heated with laser powers $\geq$ 2100 W (Fig. 11). Hence, ATR-FTIR captures the 2100 W as the critical laser power that first results in thermal degradation on the surface of CF/PEEK (Fig. 11). This value has a good agreement with the results of the numerical model that captured 2070 W as the critical laser power in the examined case study. This demonstrates the validity of the model and of the applied extrapolation approach, and to further support these findings the laser-heated samples are also examined with OM.

5.4. Optical microscopy

Fig. 12 illustrates the laser-heated region of several CF/PEEK specimens of this investigation. Similarly to the ATR-FTIR analysis, OM also captures 2100 W as the critical laser power that first triggers the thermal degradation mechanisms of CF/PEEK, and overall, thermal damage takes place when a laser power $\geq$ 2100 W is applied (Fig. 12d). To begin with, the laser-heated region of the samples processed with 1900 W and 2000 W is found similar to the surface of the virgin CF/PEEK (Fig. 12a) and no thermal damage is identified in these specimens (Fig. 12b, Fig. 12c). On the other hand, the thermal damage is apparent at an applied laser power of 2100 W (Fig. 12d) and above (Fig. 12e - Fig. 12g). To enhance this observation, Fig. 13 illustrates the boundaries of the heat-affected region of the CF/PEEK specimens heated with laser powers $\geq$ 2100 W. The laser heating effect is evident on the surface of CF/PEEK and the heat-affected region of the examined specimens can be clearly distinguished from the non-affected region (Fig. 13).

5.5. Surface morphology and surface roughness

To further assess the effect of the applied laser heating on the CF/PEEK specimens, a 3D non-contact profilometer is used to examine their surface morphology and surface roughness. In particular, the Alicona Infinite Focus SL optical system is used to examine the laser-heated and non-affected region of each sample, and areas of 2 mm by 2 mm are evaluated in each sample. To begin with, Fig. 14 illustrates the surface morphology of the examined laser-heated region of each specimen. The applied laser heating results in exposed fibres when a laser power $\geq$ 2100 W is applied on the surface of CF/PEEK (Fig. 14c - Fig. 14f). This is due to the thermal degradation of the PEEK matrix that takes place in these conditions, which gets more intense when the specimens are heated with higher laser powers.

To illustrate the effect of increased laser power, the surface roughness (R_a) of each sample is examined. All the measurements take place in the transverse direction, and the results show that increasing the applied laser power increases the surface roughness R_a on the specimens' affected surface (Fig. 15). In the samples heated at 1900 W and 2000 W, a negligible increase of 4.7 % and 8.8 % is noticed in their R_a values,

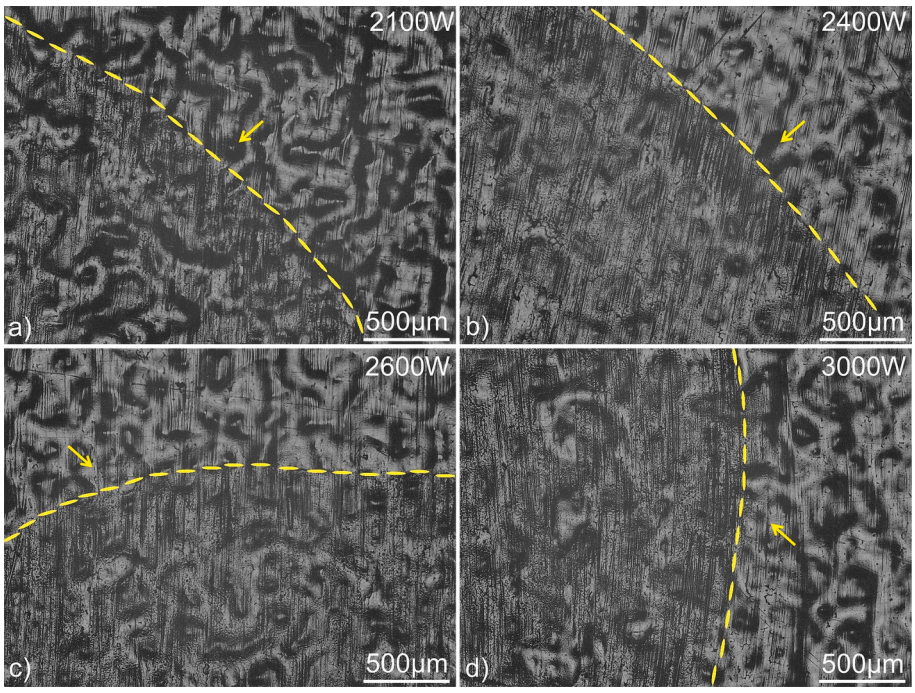

Fig. 13. Boundaries of the heat-affected region in the laser-heated CF/PEEK specimens where thermal damage occurs: (a) 2100 W, (b) 2400 W, (c) 2600 W, (d) 3000 W.

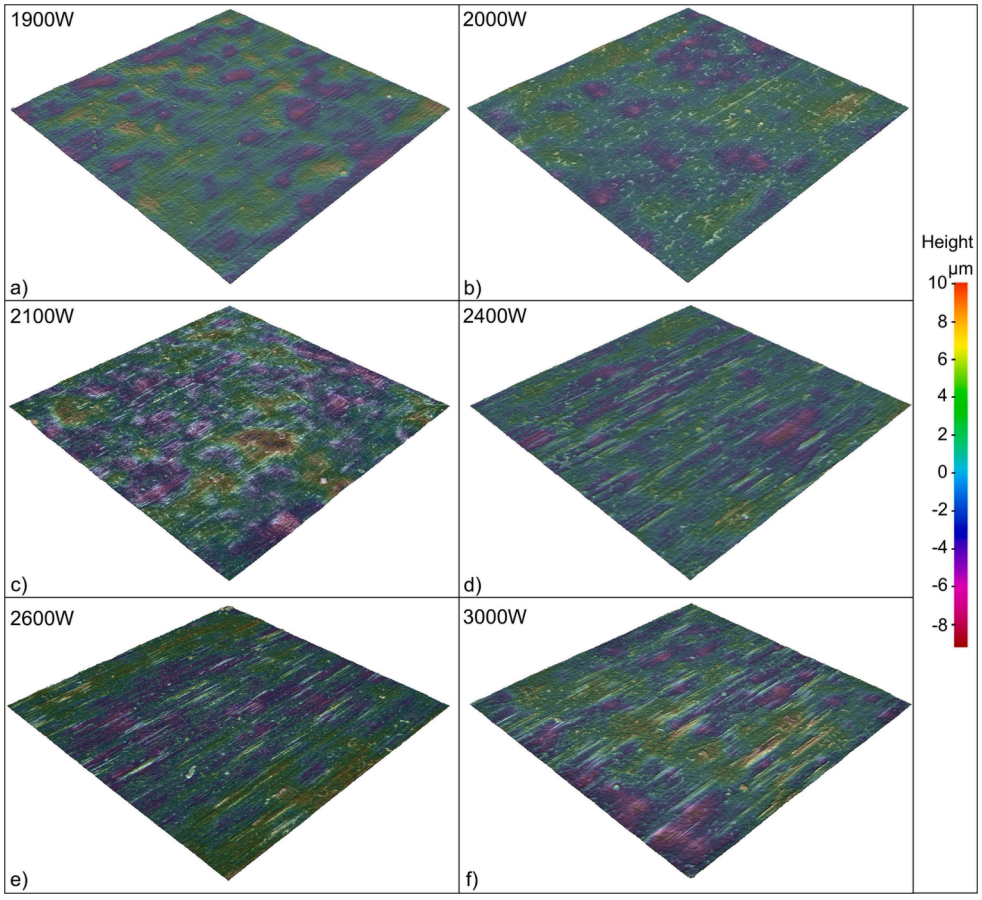

Fig. 14. Surface morphology of the laser-heated region of CF/PEEK after laser heating of 1 ms with a top-hat laser beam of 8.1 mm spot diameter, and a power of (a) 1900 W, (b) 2000 W, (c) 2100 W, (d) 2400 W, (e) 2600 W, and (f) 3000 W.

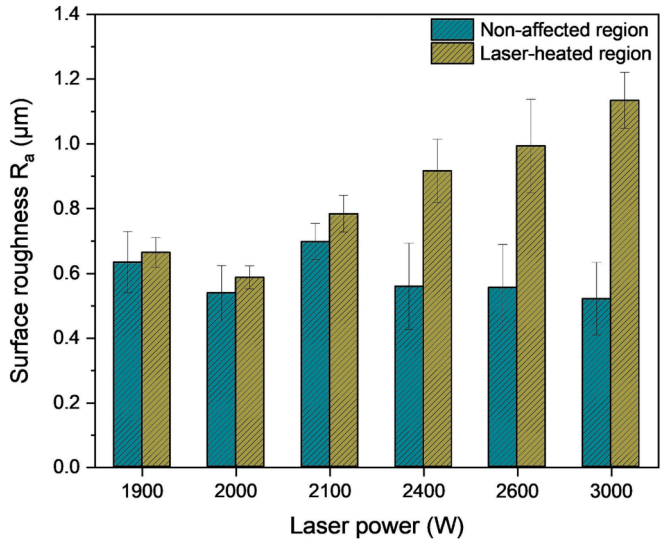

Fig. 15. Average value and standard deviation of the surface roughness R_a of the non-affected and laser-heated region of the examined specimens (transverse direction).

while a 15 % increase takes place at 2100 W with a further rise of up to 64 %, 79 %, and 179 % when the CF/PEEK samples are respectively heated with 2400 W, 2600 W, and 3000 W. This is attributed to the thermal degradation that occurs on the surface of these samples. Hence, the results clearly demonstrate the greater extent of thermal degradation on the surface of CF/PEEK heated with increased laser powers. Therefore, the surface roughness of a sample's heat-heated region could serve for characterising the extent of thermal damage after laser heating, and overall, correlating the resulting surface roughness with the extent of thermal degradation would be an interesting future investigation. This methodology could also be relevant for studies that aim to identify the resulting HAZ boundaries in several high-temperature applications of CFRPs (e.g. laser cutting, composites machining).

6. Conclusions

The present work introduced a numerical framework that employs an extrapolation approach to examine the response of CFRPs at extreme heating rates. The results showed that the model captures the effect of the heating rate on the decomposition of the examined material. Considering that the material properties are a function of the decomposition degree α, this ensures a more realistic representation of the material properties throughout the simulation compared to other methodologies that do not account for the heating rate effect.

To demonstrate the applicability of the model, a laser heating case study of CF/PEEK was examined and the process window that can achieve high-temperature processing without triggering the thermal degradation of the PEEK matrix was defined for both a Gaussian and a top-hat laser beam. To validate the model and the applied extrapolation approach, an experimental investigation also took place where the laser-heated samples were examined with ATR-FTIR, OM, and their surface roughness was also assessed.

The results showed that measuring the surface roughness could serve as a method for characterising the extent of thermal degradation that takes place in laser-heated and heat-affected CFRPs. Additionally, a very good agreement was found between the experimental and the numerical investigations and both analyses captured a similar critical laser power that first triggers the thermal degradation of CF/PEEK in the examined case study. This is an important finding, since it provides evidence for the first that the applied extrapolation approach manages to capture the onset of thermal degradation in the extreme heating conditions that take place in laser heating.

Therefore, the proposed model is a solid numerical strategy for examining the response of CFRPs at extreme heating rates, and it could be used to examine the response of a range of FRPs at these conditions with several matrix and reinforcement systems. Especially in high-temperature applications where thermal degradation could occur, the model could be employed to identify the processing conditions that would prevent these damage mechanisms. For example, it could be a useful tool to studies that aim to minimise the extent of the resulting HAZ in several high-temperature applications of FRPs, such as composite/metal laser joining, composite machining, and induction welding.

CRediT authorship contribution statement

Dimitrios Gaitanelis: Conceptualization, Methodology, Software, Validation, Formal analysis, Investigation, Resources, Data curation, Writing – original draft, Writing – review & editing, Visualization, Project administration. **Chris Worrall:** Supervision, Project administration, Resources. **Mihalis Kazilas:** Supervision, Project administration, Funding acquisition.

Declaration of competing interest

The authors declare that they have no known competing financial interests or personal relationships that could have appeared to influence the work reported in this paper.

Data availability

Data will be made available on request.

Acknowledgement

This publication was made possible by the sponsorship and support of TWI. The work was enabled through, and undertaken at, the National Structural Integrity Research Centre (NSIRC), a postgraduate engineering facility for industry-led research into structural integrity established and managed by TWI through a network of both national and international Universities.

References

[1] Tan X, Zhang J, Shan J, Yang S, Ren J. Characteristics and formation mechanism of porosities in CFRP during laser joining of CFRP and steel. Compos B Eng 2015;70:35–43. https://doi.org/10.1016/j.compositesb.2014.10.023.
[2] Lambiase F, Genna S. Laser-assisted direct joining of AISI304 stainless steel with polycarbonate sheets: thermal analysis, mechanical characterization, and bonds morphology. Opt Laser Technol 2017;88:205–14. https://doi.org/10.1016/j.optlastec.2016.09.028.
[3] Katayama S, Kawahito Y. Laser direct joining of metal and plastic. Scripta Mater 2008;59:1247–50. https://doi.org/10.1016/j.scriptamat.2008.08.026.
[4] Jung KW, Kawahito Y, Katayama S. Laser direct joining of carbon fibre reinforced plastic to stainless steel. Sci Technol Weld Join 2011;6:676–80. https://doi.org/10.1179/1362171811Y.0000000060.
[5] Jung KW, Kawahito Y, Takahashi M, Katayama S. Laser direct joining of carbon fiber reinforced plastic to aluminum alloy. J Laser Appl 2013;25. https://doi.org/10.2351/1.4794297.
[6] Mathew J, Goswami GL, Ramakrishnan N, Naik NK. Parametric studies on pulsed Nd:YAG laser cutting of carbon fibre reinforced plastic composites. J Mater Process Technol 1999;89–90:198–203. https://doi.org/10.1016/S0924-0136(99)00011-4.
[7] Li M, Gan G, Zhang Y, Yang X. Thermal defect characterization and strain distribution of CFRP laminate with open hole following fiber laser cutting process. Opt Laser Technol 2020;122:105891. https://doi.org/10.1016/j.optlastec.2019.105891.
[8] Riveiro A, Quintero F, Lusquiños F, del Val J, Comesaña R, Boutinguiza M, et al. Laser cutting of carbon fiber composite materials. Proc Manuf 2017;13:388–95. https://doi.org/10.1016/j.promfg.2017.09.026.
[9] Li M, Li S, Yang X, Zhang Y, Liang Z. Effect of lay-up configuration and processing parameters on surface quality during fiber laser cutting of CFRP laminates. Int. J. Adv. Manuf. Technol. 2019;100:623–35. https://doi.org/10.1007/s00170-018-2728-9.

[10] Li M, Gan G, Zhang Y, Yang X. Thermal damage of CFRP laminate in fiber laser cutting process and its impact on the mechanical behavior and strain distribution. Arch Civil Mech Eng 2019;19:1511–22. https://doi.org/10.1016/j.acme.2019.08.005.
[11] Clancy G, Peeters D, Oliveri V, Jones D, O'Higgins RM, Weaver PM. A study of the influence of processing parameters on steering of carbon Fibre/PEEK tapes using laser-assisted tape placement. Compos B Eng 2019;163:243–51. https://doi.org/10.1016/j.compositesb.2018.11.033.
[12] Esselink FS, Amin Hosseini SM, Baran I, Akkerman R. Optimization of laser-assisted tape winding/placement process using inverse optical model. Proc Manuf 2020;47:182–9. https://doi.org/10.1016/j.promfg.2020.04.172.
[13] Zhao D, Chen J, Zhang H, Liu W, Yue G, Pan L. Effects of processing parameters on the performance of carbon fiber reinforced polyphenylene sulfide laminates manufactured by laser-assisted automated fiber placement. J Compos Mater 2022;56:427–39. https://doi.org/10.1177/00219983211055827.
[14] Oliveri V, Zucco G, Peeters D, Clancy G, Telford R, Rouhi M, et al. Design, manufacture and test of an in-situ consolidated thermoplastic variable-stiffness wingbox. AIAA J 2019;57(4):1671–83. https://doi.org/10.2514/1.J057758.
[15] Schäkel M, Hosseini SMA, Janssen H, Baran I, Brecher C. Temperature analysis for the laser-assisted tape winding process of multi-layered composite pipes. Proc CIRP 2019;85:171–6. https://doi.org/10.1016/j.procir.2019.09.003.
[16] Kim HJ, Kim SK, Il LW. A study on heat transfer during thermoplastic composite tape lay-up process. Exp Therm Fluid Sci 1996;13:408–18. https://doi.org/10.1016/S0894-1777(96)00095-7.
[17] Stokes-Griffin CM, Compston P. An inverse model for optimisation of laser heat flux distributions in an automated laser tape placement process for carbon-fibre/PEEK. Compos Part A Appl Sci Manuf 2016;88:190–7. https://doi.org/10.1016/j.compositesa.2016.05.034.
[18] Tan C, Su J, Zhu B, Li X, Wu L, Chen Bo, et al. Effect of scanning speed on laser joining of carbon fiber reinforced PEEK to titanium alloy. Opt Laser Technol 2020;129:106273. https://doi.org/10.1016/j.optlastec.2020.106273.
[19] Mouritz AP, Feih S, Kandare E, Mathys Z, Gibson AG, Des Jardin PE, et al. Review of fire structural modelling of polymer composites. Compos Part A Appl Sci Manuf 2009;40(12):1800–14. https://doi.org/10.1016/j.compositesa.2009.09.001.
[20] Caporale AM, Airoldi A, Natali M, Boiocchi M, Torre L, Rallini M. Thermomechanical response of out-of-autoclave infused carbon-phenolic laminates for rocket engine applications subjected to surface ablation. Compos. Part A Appl. Sci. Manuf. 2022;159:107035. https://doi.org/10.1016/j.compositesa.2022.107035.
[21] Arkhurst BM, Seol JB, Lee YS, Lee M, Kim JH. Interfacial structure and bonding mechanism of AZ31/carbon-fiber-reinforced plastic composites fabricated by thermal laser joining. Compos B Eng 2019;167:71–82. https://doi.org/10.1016/j.compositesb.2018.12.002.
[22] Gaitanelis DG, Giannopoulos IK, Theotokoglou EE. Numerical FEA parametric analysis of CAI behaviour of CFRP stiffened panels. Thin-Walled Struct 2019;143:106231. https://doi.org/10.1016/j.tws.2019.106231.
[23] Villegas IF, Rubio PV. On avoiding thermal degradation during welding of high-performance thermoplastic composites to thermoset composites. Compos Part A Appl Sci Manuf 2015;77:172–80. https://doi.org/10.1016/j.compositesa.2015.07.002.
[24] Sonmez FO, Akbulut M. Process optimization of tape placement for thermoplastic composites. Compos Part A Appl Sci Manuf 2007;38:2013–23. https://doi.org/10.1016/j.compositesa.2007.05.003.
[25] Xia H, Ma Y, Chen C, Su J, Zhang C, Tan C, et al. Influence of laser welding power on steel/CFRP lap joint fracture behaviors. Compos Struct 2022;285:115247. https://doi.org/10.1016/j.compstruct.2022.115247.
[26] Cepero-Mejías F, Curiel-Sosa JL, Blázquez A, Yu TT, Kerrigan K, Phadnis VA. Review of recent developments and induced damage assessment in the modelling of the machining of long fibre reinforced polymer composites. Compos Struct 2020;240:112006. https://doi.org/10.1016/j.compstruct.2020.112006.
[27] Seward O, Cepero-Mejías F, Fairclough JPA, Kerrigan K. Development of a Novel Friction Model for Machining Simulations in Unidirectional Composite Materials. Polymers 2022;14(5):847. https://doi.org/10.3390/polym14050847.
[28] Stokes-Griffin CM, Compston P. A combined optical-thermal model for near-infrared laser heating of thermoplastic composites in an automated tape placement process. Compos Part A Appl Sci Manuf 2015;75:104–15. https://doi.org/10.1016/j.compositesa.2014.08.006.
[29] Hosseini SMA, Baran I, van Drongelen M, Akkerman R. On the temperature evolution during continuous laser-assisted tape winding of multiple C/PEEK layers: The effect of roller deformation. Int J Mater Form 2021;14(2):203–21. https://doi.org/10.1007/s12289-020-01568-7.
[30] Stokes-Griffin CM, Compston P, Matuszyk TI, Cardew-Hall MJ. Thermal modelling of the laser-assisted thermoplastic tape placement process. J Thermoplast Compos Mater 2015;28:1445–62. https://doi.org/10.1177/0892705713513285.
[31] Su J, Tan C, Wu Z, Wu L, Gong X, Chen Bo, et al. Influence of defocus distance on laser joining of CFRP to titanium alloy. Opt Laser Technol 2020;124:106006. https://doi.org/10.1016/j.optlastec.2019.106006.
[32] Canel T, Bağlan İ, Sınmazçelik T. Mathematical modeling of heat distribution on carbon fiber Poly(ether-ether-ketone) (PEEK) composite during laser ablation. Opt Laser Technol 2020;127:106190. https://doi.org/10.1016/j.optlastec.2020.106190.
[33] Day M, Cooney JD, Wiles DM. The kinetics of the oxidative degradation of poly (aryl-ether-ether-ketone) (PEEK). Thermochim Acta 1989;147:189–97. https://doi.org/10.1016/0040-6031(89)85174-3.
[34] Gaitanelis D, Worrall C, Kazilas M. Detecting, characterising and assessing PEEK's and CF-PEEK's thermal degradation in rapid high-temperature processing. Polym Degrad Stab 2022;204:110096. https://doi.org/10.1016/j.polymdegradstab.2022.110096.
[35] Dong Q, Guo Y, Sun X, Jia Y. Coupled electrical-thermal-pyrolytic analysis of carbon fiber/epoxy composites subjected to lightning strike. Polymer (Guildf) 2015;56:385–94. https://doi.org/10.1016/j.polymer.2014.11.029.
[36] Guo Y, Dong Q, Chen J, Yao X, Yi X, Jia Y. Comparison between temperature and pyrolysis dependent models to evaluate the lightning strike damage of carbon fiber composite laminates. Compos Part A Appl Sci Manuf 2017;97:10–8. https://doi.org/10.1016/j.compositesa.2017.02.022.
[37] Dong Q, Guo Y, Chen J, Yao X, Yi X, Ping L, et al. Influencing factor analysis based on electrical–thermal-pyrolytic simulation of carbon fiber composites lightning damage. Compos Struct 2016;140:1–10. https://doi.org/10.1016/j.compstruct.2015.12.033.
[38] Kamiyama S, Hirano Y, Ogasawara T. Delamination analysis of CFRP laminates exposed to lightning strike considering cooling process. Compos Struct 2018;196:55–62. https://doi.org/10.1016/j.compstruct.2018.05.003.
[39] Wan G, Dong Q, Zhi J, Guo Y, Yi X, Jia Y. Analysis on electrical and thermal conduction of carbon fiber composites under lightning based on electrical-thermal-chemical coupling and arc heating models. Compos Struct 2019;229:111486. https://doi.org/10.1016/j.compstruct.2019.111486.
[40] Millen SLJ, Ashworth S, Farrell C, Murphy A. Understanding and representing heating and heating rate effects on composite material properties for lightning strike direct effect simulations. Compos B Eng 2022;228:109438. https://doi.org/10.1016/j.compositesb.2021.109438.
[41] Abaqus/Standard User's Manual, Version 6.14. Simulia; 2014.
[42] Wang Y. Multiphysics analysis of lightning strike damage in laminated carbon/glass fiber reinforced polymer matrix composite materials: a review of problem formulation and computational modeling. Compos Part A Appl Sci Manuf 2017;101:543–53. https://doi.org/10.1016/j.compositesa.2017.07.010.
[43] Foster P, Abdelal G, Murphy AP. Understanding how arc attachment behaviour influences the prediction of composite specimen thermal loading during an artificial lightning strike test. Compos Struct 2018;192:671–83. https://doi.org/10.1016/j.compstruct.2018.03.039.
[44] Abdelal G, Murphy AP. Nonlinear numerical modelling of lightning strike effect on composite panels with temperature dependent material properties. Compos Struct 2014;109:268–78. https://doi.org/10.1016/j.compstruct.2013.11.007.
[45] Patel P, Hull TR, Lyon RE, Stoliarov SI, Walters RN, Crowley S, et al. Investigation of the thermal decomposition and flammability of PEEK and its carbon and glass-fibre composites. Polym Degrad Stab 2011;96:12–22. https://doi.org/10.1016/j.polymdegradstab.2010.11.009.
[46] Henderson JB, Tant MR, Moore GR, Wiebelt JA. Determination of kinetic parameters for the thermal decomposition of phenolic ablative materials by a multiple heating rate method. Thermochim Acta 1981;44:253–64. https://doi.org/10.1016/0040-6031(81)85019-8.
[47] Hildenwall B, Ericsson T. Prediction of residual stresses in case-hardening steels [C]. Hardenability Concepts with applications to Steel, Warrendale. TMS-AIME 1977:579–606.
[48] Vyazovkin S, Burnham AK, Criado JM, Pérez-Maqueda LA, Popescu C, Sbirrazzuoli N. ICTAC Kinetics Committee recommendations for performing kinetic computations on thermal analysis data. Thermochim Acta 2011;520:1–19. https://doi.org/10.1016/j.tca.2011.03.034.
[49] Gaitanelis D, Chanteli A, Worrall C, Weaver PM, Kazilas M. A multi-technique and multi-scale analysis of the thermal degradation of PEEK in laser heating. Polym Degrad Stab 2023;211:110282. https://doi.org/10.1016/j.polymdegradstab.2023.110282.
[50] Flynn JH, Wall LA. A quick, direct method for the determination of activation energy from thermogravimetric data. J Polym Sci B 1966;4:323–8. https://doi.org/10.1002/pol.1966.110040504.
[51] ASTM E1641-16. Standard Test Method for Decomposition Kinetics by Thermogravimetry Using the Ozawa/Flynn/Wall Method n.d.
[52] Millen SLJ, Murphy A, Catalanotti G, Abdelal G. Coupled thermal-mechanical progressive damage model with strain and heating rate effects for lightning strike damage assessment. Appl Compos Mater 2019;26:1437–59. https://doi.org/10.1007/s10443-019-09789-z.
[53] Rawal SP, Misra MS. Measurement of mechanical and thermophysical properties of dimensionally stable materials for space applications. NASA Contract Rep 1992.
[54] Cogswell FN, editor. Subject Index. Thermoplastic Aromatic Polymer Composites, Butterworth-Heinemann; 1992, p. 263–8. https://doi.org/10.1016/B978-0-7506-1086-5.50037-9.
[55] Griffis CA, Nemes JA, Stonesifer FR, Chang CI. Degradation in strength of laminated composites subjected to intense heating and mechanical loading. J Compos Mater 1986;20:216–35. https://doi.org/10.1177/002199838602000301.
[56] Fanucci JP. Thermal response of radiantly heated Kevlar and graphite/epoxy composites. J Compos Mater 1987;21:129–39. https://doi.org/10.1177/002199838702100204.
[57] Tant MR, Henderson JB, Boyer CT. Measurement and modelling of the thermochemical expansion of polymer composites. Composites 1985;16:121–6. https://doi.org/10.1016/0010-4361(85)90618-4.
[58] Kamiyama S, Hirano Y, Okada T, Ogasawara T. Lightning strike damage behavior of carbon fiber reinforced epoxy, bismaleimide, and polyetheretherketone composites. Compos Sci Technol 2018;161:107–14. https://doi.org/10.1016/j.compscitech.2018.04.009.
[59] Chanteli A, Bandaru AK, Peeters D, O'Higgins RM, Weaver PM. Influence of repass treatment on carbon fibre-reinforced PEEK composites manufactured using laser-

assisted automatic tape placement. Compos Struct 2020;248:112539. https://doi.org/10.1016/j.compstruct.2020.112539.
[60] Papkov VS, Gerasimov MV, Dubovik II. Disordering of crystalline PEEK upon mechanical treatment. Polym Eng Sci 1997;37:1280–5. https://doi.org/10.1002/pen.11773.
[61] Ray D, Comer AJ, Lyons J, Obande W, Jones D, Higgins RMO, et al. Fracture toughness of carbon fiber/polyether ether ketone composites manufactured by autoclave and laser-assisted automated tape placement. J Appl Polym Sci 2015;132(11). https://doi.org/10.1002/app.41643.
[62] Dolo G, Férec J, Cartié D, Grohens Y, Ausias G. Model for thermal degradation of carbon fiber filled poly(ether ether ketone). Polym Degrad Stab 2017;143:20–5. https://doi.org/10.1016/j.polymdegradstab.2017.06.006.
[63] Colak ZS, Sonmez FO, Kalenderoglu V. Process modeling and optimization of resistance welding for thermoplastic composites. J Compos Mater 2002;36:721–44. https://doi.org/10.1177/0021998302036006507.
[64] Sonmez FO, Hahn HT. Modeling of heat transfer and crystallization in thermoplastic composite tape placement process. J Thermoplast Compos Mater 1997;10:198–240. https://doi.org/10.1177/089270579701000301.
[65] Allison SW, Gillies GT. Remote thermometry with thermographic phosphors: Instrumentation and applications. Rev. Sci. Instrum. 1997;68(7):2615–50. https://doi.org/10.1063/1.1148174.
[66] Vetter TM, Bibinger J, Zimmer F, Eibl S, Gudladt H-J. Characterization of one-sided thermal damage of carbon fiber reinforced polymers by means of depth profiles. J. Compos. Mater. 2020;54(24):3699–713. https://doi.org/10.1177/0021998320917190.
[67] Bartolucci SF, Supan KE, Warrender JM, Davis CE, Beaud LL, Knowles K, et al. Laser-induced thermo-oxidative degradation of carbon nanotube/polypropylene nanocomposites. Compos Sci Technol 2014;105:166–73. https://doi.org/10.1016/j.compscitech.2014.09.018.
[68] Al Lafi AG. FTIR spectroscopic analysis of ion irradiated poly (ether ether ketone). Polym Degrad Stab 2014;105:122–33. https://doi.org/10.1016/j.polymdegradstab.2014.04.005.
[69] Pascual A, Toma M, Tsotra P, Grob MC. On the stability of PEEK for short processing cycles at high temperatures and oxygen-containing atmosphere. Polym Degrad Stab 2019;165:161–9. https://doi.org/10.1016/j.polymdegradstab.2019.04.025.